analytica

MDPI

Article

Characterization of Multi-Pass Enhanced Raman Spectroscopy for Gaseous Measurement

Miao Fan, Huinan Yang and Jun Chen *

School of Energy and Power Engineering, University of Shanghai for Science and Technology, Shanghai 200093, China
* Correspondence: j.chen@usst.edu.cn

Abstract: With the rise in global temperatures, it is of great significance to achieve rapid and accurate detection of greenhouse gases, such as carbon dioxide and methane. Raman spectroscopy not only overcomes the weakness of absorption spectroscopy in simultaneously measuring homonuclear diatomic molecules but also enables the simultaneous detection of multiple gases using a single-wavelength laser. However, due to the small Raman scattering cross-section and weak intensity of molecules, its application in gas detection is limited. To enhance the intensity of Raman scattering, this paper designs and constructs a multi-pass enhanced Raman spectroscopy setup. This study focuses on the effects of Raman scattering collection geometry, laser multi-pass patterns, and laser polarization relative to the Raman collection direction on signal intensity. Investigations into Raman scattering collection angles of 30°, 60°, and 90° reveal that the Raman scattering signal intensity increases as the collection angle decreases. Different laser multi-pass patterns also impact the signal, with the near-concentric linear multi-pass pattern found to collect more signals. To minimize the influence of excitation light on the signal, a side collection system is employed. Experiments show that the Raman scattering signal is stronger when the laser polarization is perpendicular to the collection direction. This study achieves overall system performance enhancement through coordinated optimization of multiple physical mechanisms, including Raman scattering collection geometry, laser multi-pass patterns, and laser polarization characteristics. The optimized setup was employed to characterize the laser power dependence for nitrogen, oxygen, and carbon dioxide detection. The results showed that the Raman scattering intensity varied linearly with the laser power of the gases, with linear fitting goodness R^2 values of 0.9902, 0.9848, and 0.9969, respectively. Finally, by configuring different concentrations of carbon dioxide gas using nitrogen, it was found that the Raman scattering intensity varied linearly with the concentration of carbon dioxide, with a linear fitting goodness R^2 of 0.9812. The system achieves a CO_2 detection limit of 500 ppm at 200 s integration time, meeting the requirements for greenhouse gas emission monitoring applications.

Keywords: Raman spectroscopy; gas detection; multi-pass cavity

check for updates

Academic Editors: Fotouh Rashed, Marcello Locatelli and Alaa Bedair

Received: 17 March 2025
Revised: 6 April 2025
Accepted: 11 April 2025
Published: 16 April 2025

Citation: Fan, M.; Yang, H.; Chen, J. Characterization of Multi-Pass Enhanced Raman Spectroscopy for Gaseous Measurement. *Analytica* **2025**, *6*, 13. https://doi.org/10.3390/analytica6020013

Copyright: © 2025 by the authors. Licensee MDPI, Basel, Switzerland. This article is an open access article distributed under the terms and conditions of the Creative Commons Attribution (CC BY) license (https://creativecommons.org/licenses/by/4.0/).

1. Introduction

As global environmental pollution issues become increasingly severe, climate change has emerged as a significant challenge for humanity. China has proposed the goals of "carbon peak" and "carbon neutrality", aiming to reduce greenhouse gas emissions and promote a green, low-carbon transformation. In this process, it is crucial to accurately monitor greenhouse gases, such as carbon dioxide and methane, and harmful gases from

industrial emissions. However, spectroscopic gas sensing technology has always been a popular yet challenging subject. Among the most commonly used methods are those based on infrared absorption, including direct infrared absorption spectroscopy [1], photoacoustic spectroscopy [2], and cavity ring-down spectroscopy [3]. These techniques have large absorption cross-sections, high sensitivity, and good selectivity. However, they struggle to simultaneously detect homonuclear diatomic molecules, such as N_2, H_2, O_2, etc., which are particularly relevant in many fields, including biology [4], human disease detection [5], and environmental science [6]. Different gases have different absorption wavelengths, necessitating the use of lasers of various wavelengths for the detection of multi-component gases. Additionally, water absorption can significantly impact detection due to its substantial footprint in the infrared window, making it difficult for these techniques to detect the presence of analytes at very low concentrations.

In 1923, Adolf Smekal predicted the phenomenon of Raman scattering [7], which was experimentally verified by C.V. Raman and K.S. Krishnan in 1928 [8]. Raman spectroscopy [9,10] is based on the Raman scattering effect of substances [11], which serves as a molecular fingerprint, enabling the detection of almost all molecules (except for monatomic molecules), including homonuclear diatomic molecules. Moreover, it allows for the simultaneous and rapid detection of multi-component gases using a single-wavelength laser. However, due to the small Raman scattering cross-section, gaseous detection is limited.

In recent years, researchers, both domestically and internationally, have employed various enhancement methods to improve the detection sensitivity of Raman scattering, such as Surface-Enhanced Raman Spectroscopy (SERS) [12], Coherent Anti-Stokes Raman Spectroscopy (CARS) [13], and Fiber-Enhanced Raman Spectroscopy (FERS) [14]. These methods indicate that enhancing Raman spectroscopy requires the pre-treatment of samples, and the measurement results are significantly affected by the substrate, leading to poor reproducibility. Coherent Anti-Stokes Raman Spectroscopy requires a second tunable laser source, resulting in higher costs and more sophisticated setups; Fiber-Enhanced Raman Spectroscopy is influenced by the different bending losses of optical fibers in various curved states; thus, the Raman scattering intensity of gases can be affected by the placement of the fiber. Another method to enhance Raman scattering intensity is cavity-enhanced Raman spectroscopy (CERS) [15–17]; this is a non-destructive optical detection technique capable of performing highly sensitive detection of emitted gases. Based on different optical cavity structures, including multi-pass cavities [18–21], F-P cavities [22], microcavities [23], etc., Juan [24] et al. employed a near-concentric bidirectional multi-pass cell to boost the circulating power of a blue multimode laser diode (443 nm) to approximately 100 W, significantly enhancing the gas-phase Raman signal. Under 100 s integration, this system achieved a detection limit of 8.6 ppm for carbon dioxide.

For cavity-enhanced Raman spectroscopy, the Raman scattering intensity exhibits the following angular dependence [25]:

$$I_k = \left[\frac{\langle Q_{k0} \rangle (\omega_0 \mp \omega_k)^4}{32\pi c^3} \left(2\pi - \pi \sin^2 \gamma \right) \right] \left| \alpha'_k \cdot E_0 \right|^2 \quad (1)$$

Q_{k0} represents the vibrational coordinate, w_0 is the excitation light frequency, w_k denotes the Raman shift, c stands for the speed of light, γ is the angle between the scattering direction and the dipole moment, α'_k is the derived polarizability for vibration k (where $\alpha'_k \neq 0$ indicates Raman activity), and E_0 is the electric field strength of the excitation light. According to Equation (1), the Raman scattering intensity is maximized in either the forward ($\gamma = 0°$) or backward ($\gamma = 180°$) scattering directions and minimized in the side-scattering ($\gamma = 90°$) geometry.

Currently, spectroscopic methods capable of achieving high-sensitivity detection of greenhouse gases include cavity ring-down spectroscopy (CRDS). For instance, the Picarro greenhouse gas analyzer, available on the market and based on the principle of CRDS, can achieve measurement precision at the parts-per-billion (ppb) level for greenhouse gases. However, CRDS cannot simultaneously detect multiple gases using a single-wavelength laser. On the other hand, methods that offer lower sensitivity for greenhouse gas measurements include electrochemical sensor methods and non-dispersive infrared spectroscopy (NDIR), with measurement ranges typically spanning from hundreds to thousands of parts per million (ppm). Nevertheless, there remains a significant demand for medium-to-high precision greenhouse gas detection methods that bridge the gap between these two extremes. This paper introduces a medium-to-high precision, multi-pass enhanced Raman spectroscopy method and provides an in-depth discussion of its optical performance characterization.

2. Experimental Setup

Figure 1 shows a schematic diagram of the multi-pass enhanced Raman spectroscopy system. It primarily consists of four components: a laser, a multi-pass cavity, a signal collection part, and a signal detection part. Lasers are chosen as the excitation light source due to their advantages of high monochromaticity and intensity. Since the intensity of Raman scattering signals is inversely proportional to the fourth power of the wavelength and directly proportional to the excitation light power, a laser with a shorter wavelength and higher energy is used in this experiment to enhance the Raman signal intensity. A semiconductor 532 nm laser (MGL-S-532–300mW, CNI, Changchun, China) was adopted in the experiment setup. The excitation light first passes through a half-wave plate, changing the laser's polarization from horizontal to vertical, as the strongest Raman signal can be collected when the polarization direction is perpendicular to the Raman scattering collection direction [26]. The polarized light is then focused on the center of the multi-pass cavity by lens F1. Given that the plano-concave mirrors used in the experiment have a curvature radius of 100 mm, a lens with a larger focal length than the mirror's curvature radius (F1 = 200 mm) is chosen to avoid affecting the laser's reflection within the cavity. The multi-pass cavity has a simple structure, typically consisting of two plano-concave mirrors. The laser enters the cavity from the side at a certain angle and undergoes multiple reflections back and forth between the front and rear mirrors along different paths. Each reflection of the laser passes nearly through the same point within the multi-pass cavity, where interference occurs, enhancing the laser power and thereby increasing the Raman signal. The distance between the two plano-concave one-inch mirrors is 200 mm. The mirror reflectivity is greater than 99%, and the focal length of 50 mm. The light signal focused at the cavity center is collected by a telescope system consisting of two one-inch lenses (F2 = 30 mm, F3 = 100 mm), with a long-pass filter (Semrock BLP01-532R-25, Semrock, Rochester, NY, USA) placed between the lenses to eliminate the influence of excitation light and Rayleigh scattering on the signal. The collected light directly focuses on the monochromator's entrance slit; then, it is dispersed by the grating and captured by a CCD detector. The monochromator (Andor SR-303i-B, Andor Technology, Belfast, Ireland) employs a grating with a blaze wavelength of 500 nm and 600 L/mm rulings with a camera (Andor DH334T-18U-E3, Andor Technology, Belfast, Ireland) featuring a CCD matrix size of 1024 × 1024. The CCD camera was cooled to −25 °C to minimize the impact of dark current on the signal, and all experiments were carried out in a dark environment.

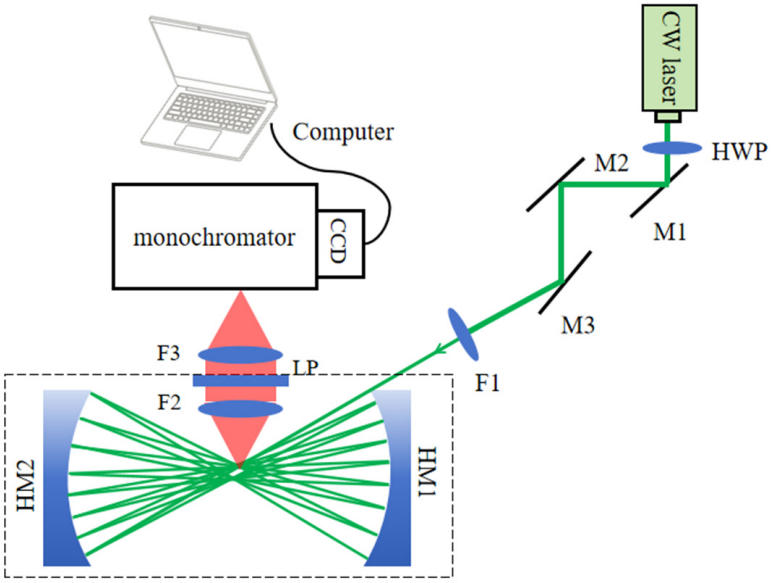


Figure 1. Schematic diagram of the multi-pass enhanced Raman spectroscopy system.

3. Results and Discussion

The multi-pass enhanced Raman spectroscopy gas detection setup constructed in this study was first used to detect the Raman signals of ambient air. The detection was performed with a 90° Raman scattering collection angle, a laser power of 300 mW, an integration time of 200 s, an entrance slit width of 100 μm, and a laboratory temperature of 25 °C. As shown in Figure 2, the Raman spectra of nitrogen (2331 cm^{-1}) and oxygen (1554 cm^{-1}) in the air are presented. The nitrogen content in the air is 78%, and the oxygen content is 21%. The presence of these two characteristic Raman peaks is clearly observed. In greenhouse gas monitoring research, all measurements are conducted against the background of the atmospheric environment. Nitrogen and oxygen, due to their stable concentrations and distinct Raman characteristic peaks, serve as ideal references for correcting system fluctuations. This study validates the universality of the multi-pass cell through the detection of conventional gases, laying the foundation for subsequent measurements of the greenhouse gas carbon dioxide. More importantly, this technology enables the simultaneous detection of multiple gas components using single-wavelength excitation, demonstrating its unique advantages in analyzing complex atmospheric compositions.

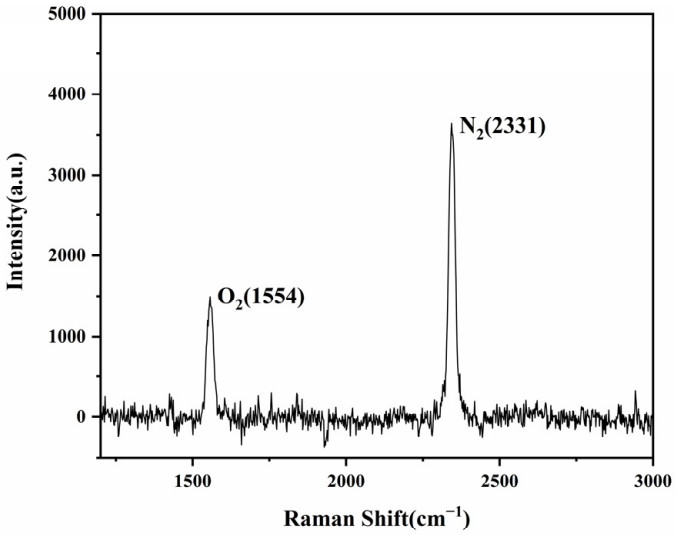


Figure 2. Raman signal intensity of oxygen and nitrogen in ambient air.

3.1. Optimization of Raman Scattering Collection Geometry

According to Equation (1), the Raman scattering signal intensity exhibits angular dependence. Therefore, this section investigates and analyzes the influence of signal collection angles on Raman scattering signals. Figure 3 shows Raman signal intensity characterization at three collection geometries. Figure 3a shows a schematic diagram of the Raman scattering collection geometry, where the angle between the optical axis direction and the collection direction is θ. Through the systematic characterization of the Raman scattering collection geometries (30°, 60°, 90°), we observed a significant angular dependence on signal intensity (Figure 3b). It was found that as the collection geometry θ decreases, the Raman scattering intensity gradually increases, with the lowest intensity at 90° collection and the strongest at 30° collection. The 30°collection configuration demonstrated a 7-fold enhancement compared to conventional 90° backscattering geometry. This critical finding establishes that oblique angle collection effectively amplifies the detection of weak Raman signals, providing a key design principle for sensitive gas-phase Raman spectroscopy systems. Therefore, a 30° collection geometry was chosen for this study.

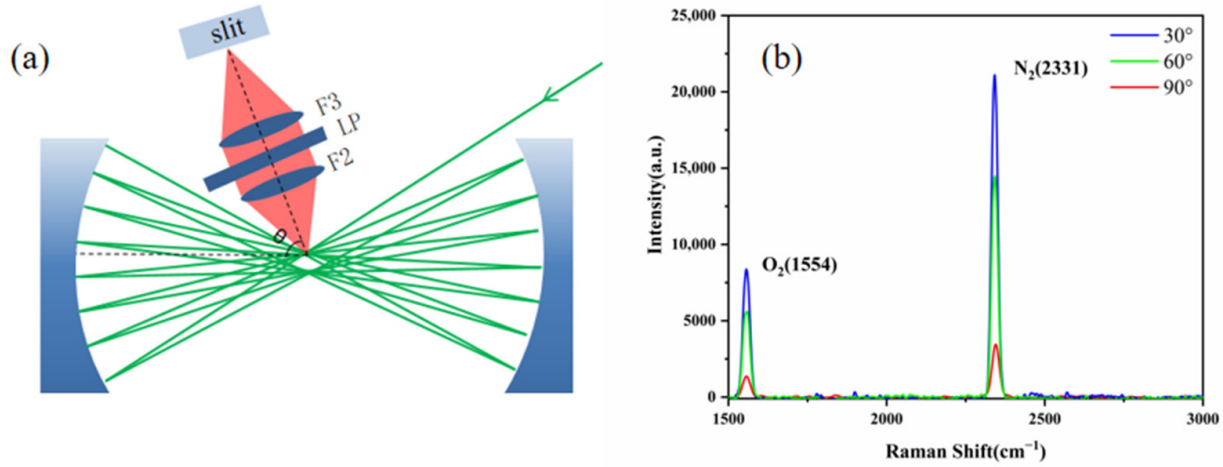


Figure 3. Raman signal intensity characterization at three collection geometries. (**a**) Schematic diagram of Raman scattering collection geometry; (**b**) Raman spectra.

3.2. Laser Multi-Pass Pattern Optimization

The intensity of Raman scattering signals is not only related to the signal collection geometry but also to the reflection pattern of the excitation laser. During the debugging process, it was found that changing the distance between the cavity mirrors or the angle between them forms different reflection patterns. Three distinct multi-pass cavity configurations were evaluated (Figure 4a–c), which, respectively, represent the near-concentric linear type, near-concentric elliptical type, and concentric linear type reflection patterns. The near-concentric linear configuration exhibited superior signal enhancement, achieving nitrogen signal intensities exceeding 20,000 counts—3–5 times greater than alternative configurations (Figure 4d). This enhancement mechanism stems from constructive interference effects at the common focal region, where multi-pass reflections create a localized high-intensity excitation zone. Notably, our experimental validation revealed that path-length optimization through cavity alignment plays a more significant role than the total reflection count. Therefore, the near-concentric linear type reflection pattern was chosen for the measurements.

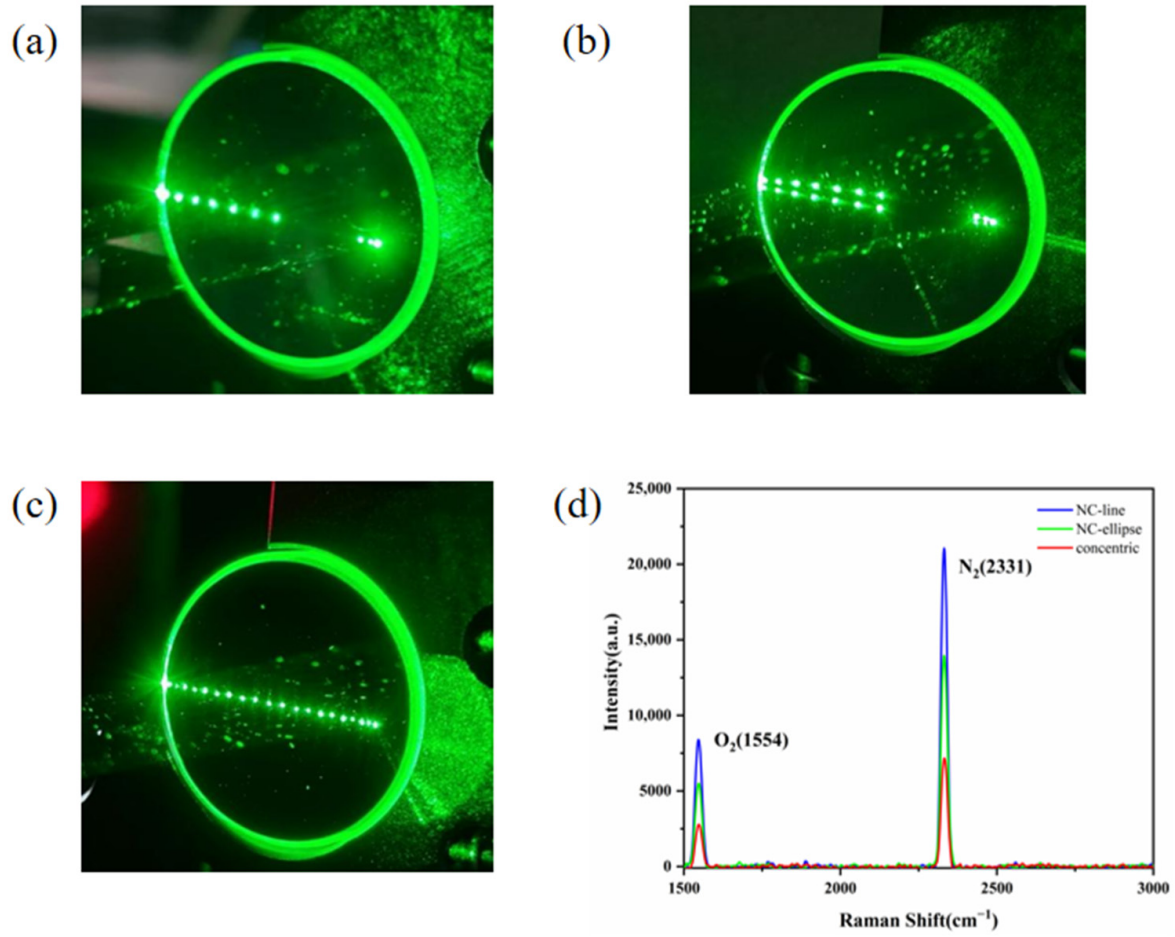


Figure 4. Characterization of excitation light multi-pass pattern. (**a**) Near-concentric linear; (**b**) near-concentric elliptical; (**c**) concentric linear; (**d**) Raman spectra.

3.3. Polarization-Dependent Signal Enhancement

Figure 5a shows the collection direction of Raman scattered light. When the collection direction is forward or backward, regardless of the laser polarization direction, it is always perpendicular to the Raman signal collection direction; thus, there is no need to adjust the laser's polarization direction. When the collection direction is lateral, the laser's polarization direction needs to be adjusted to be perpendicular to the Raman signal collection direction. Forward collection at 0° faces significant interference from the excitation light. The intensity of Rayleigh scattering from the laser can be up to 10^6 times stronger than the Raman signal. When the laser energy is high, forward collection would require the use of additional or higher optical density (OD) filters, leading to increased costs. For a multi-pass cavity, the laser beam undergoes multiple reflections and converges at a single point or a specific region within the cavity, where the Raman signal is enhanced. Therefore, sideward collection is more suitable in this configuration, as it improves the signal-to-noise ratio (SNR) while avoiding strong laser interference. The laser used in the experiment is horizontally polarized, and a half-wave plate is used to change the polarization direction from horizontal to vertical. By implementing a side collection geometry with controlled polarization alignment, a 32% signal enhancement was achieved compared to uncontrolled polarization states (Figure 5b). This improvement aligns with the theoretical predictions. Our quantitative analysis confirms that proper polarization management is crucial for background suppression in weak signal detection.

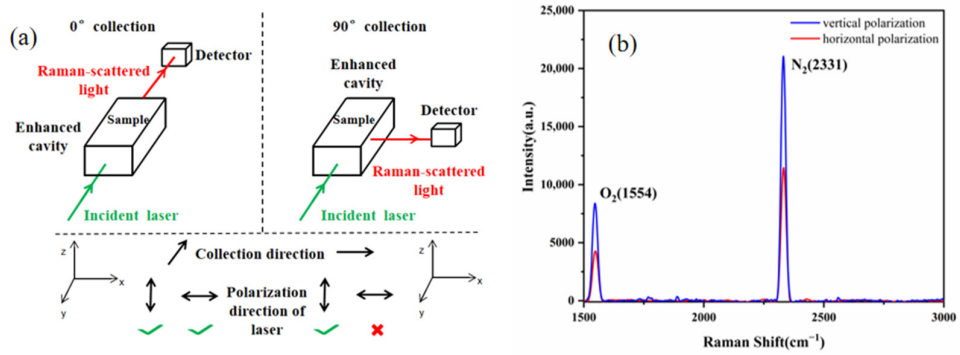


Figure 5. Laser polarization characterization. (**a**) Collection direction of Raman-scattered light; (**b**) Raman spectra.

3.4. Laser Power Linearity Characterization

Based on the constructed multi-pass enhanced Raman spectroscopy setup, this paper investigates the Raman scattering intensity of nitrogen, oxygen, and carbon dioxide in ambient air under different laser powers, with the laser power ranging from 50 mW to 300 mW, an integration time of 200 s, an entrance slit width of 100 μm, and a temperature of 25 °C. Figure 6a shows the Raman spectra of nitrogen and oxygen under different laser powers, with the Raman characteristic peak of nitrogen located at 2331 cm^{-1} and that of oxygen at 1554 cm^{-1}. The intensity of their Raman characteristic peaks varies with laser power, as shown in Figure 6b. It can be observed that the height of their Raman peaks changes linearly with laser power. Figure 6c presents the Raman spectra of carbon dioxide under different laser powers, with the Raman characterization peak of carbon dioxide located at 1388 cm^{-1}, and the intensity of its Raman characteristic peak varying with laser power, as illustrated in Figure 6d. It is evident that the height of the characteristic Raman peak of carbon dioxide changes linearly with laser power.

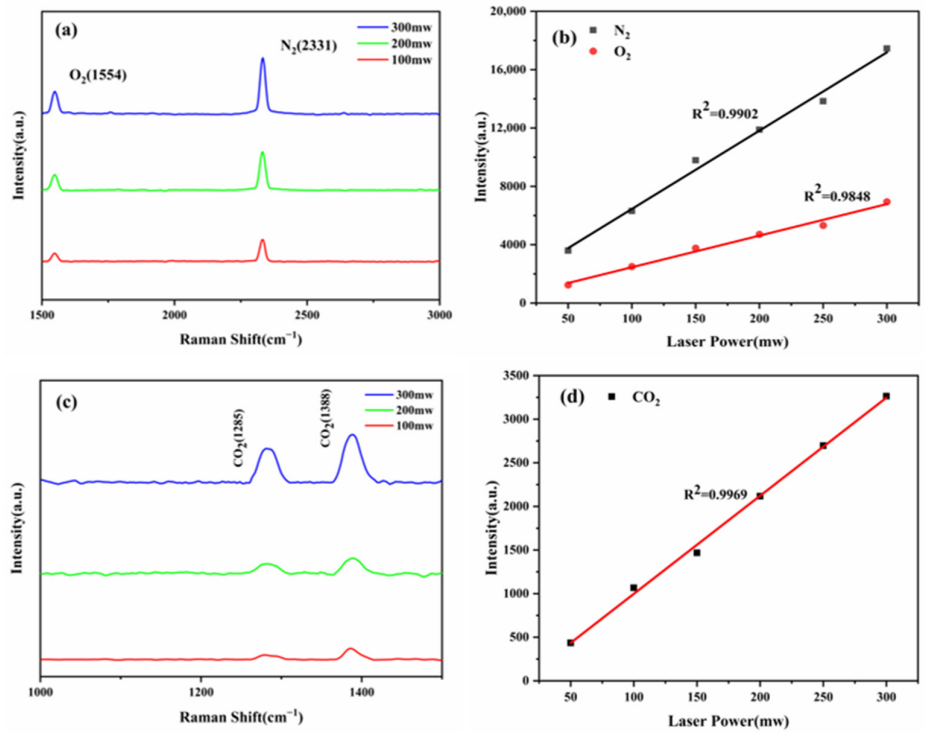


Figure 6. Laser power linearity characterization. (**a**) Raman spectra of nitrogen and oxygen; (**b**) variation of nitrogen and oxygen peak intensity with laser power; (**c**) Raman spectra of carbon dioxide; (**d**) variation of carbon dioxide peak intensity with laser power.

3.5. Concentration Calibration Performance

Based on the constructed multi-pass enhanced Raman spectroscopy setup, this paper investigates the Raman scattering intensity of carbon dioxide at various concentrations. Different concentrations of carbon dioxide gas were prepared by mixing with nitrogen (99%). The flow rate of carbon dioxide was regulated at 5 L·min^{-1} using a float flow meter, and the Raman signal intensity of carbon dioxide was studied at nitrogen flow rates of 1, 2, 3, 4, and 5 L·min^{-1}. Figure 7a presents the Raman spectra of carbon dioxide at different concentrations, with two primary Raman characteristic peaks observed at 1285 cm^{-1} and 1388 cm^{-1}. The intensity of these Raman characteristic peaks of carbon dioxide as a function of concentration is illustrated in Figure 7b. It is evident that the height of the characteristic Raman peaks of carbon dioxide varies linearly with concentration. This linear dynamic response confirms our system's potential for ppm-level quantitative analysis with proper calibration protocols.

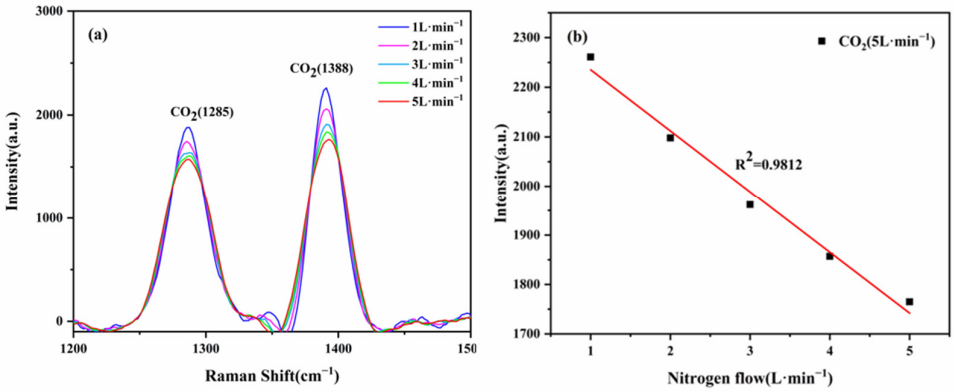


Figure 7. Concentration calibration performance of carbon dioxide. (**a**) Raman spectrum; (**b**) the intensity of Raman scattering varies with carbon dioxide concentration.

3.6. Discussion

Compared to Surface-Enhanced Raman Spectroscopy (SERS), multi-pass enhanced Raman spectroscopy eliminates substrate interference, improving repeatability by over 90% (with all results averaged over three trials), while enabling simultaneous detection of multiple gas species using a single laser source. In contrast to the collinear detection method employed in Juan's study "Trace gas sensing using diode-pumped collinearly detected spontaneous Raman scattering enhanced by a multi-pass cell", this approach avoids interference from strong pump laser reflections and scattered light, significantly reducing background noise. It also simplifies optical design by requiring only a single long-pass filter in the detection path to block residual pump light, eliminating the need for complex coaxial filtering systems. While multi-pass enhanced Raman spectroscopy significantly improves detection performance, evaluating its sensitivity is equally crucial. The detection limit for carbon dioxide is calculated to be 500 ppm.

As a completely non-contact and label-free optical detection method, the apparatus exhibits three distinctive green features compared to existing enhancement techniques: (1) the elimination of noble metal nanomaterials used in conventional Surface-Enhanced Raman Spectroscopy, thereby completely avoiding potential chemical contamination risks; (2) an all-optical cavity design that overcomes fiber-optic limitations, enabling adaptation to diverse environmental monitoring scenarios; (3) signal enhancement achieved solely through physical approaches, including extended light–gas interaction pathlength and optimized excitation field distribution, without requiring any chemical modifiers. Particularly noteworthy is that through the coordinated optimization of multiple physical mechanisms, the system maintains exceptional environmental friendliness while simultaneously deliver-

ing rapid responses and multi-component detection capabilities. This work provides new insights for developing green gas analysis technologies, offering a sustainable alternative to conventional detection methods.

4. Conclusions

In response to the need for environmentally friendly gas monitoring, this study designed and constructed a near-concentric, multi-pass cavity-enhanced Raman spectroscopy system. This study focuses on achieving comprehensive system performance enhancement through the synergistic optimization of multiple physical mechanisms, including Raman scattering collection geometry, laser multi-pass patterns, and laser polarization characteristics. The experimental results demonstrate that this technology enables highly sensitive detection of N_2, O_2, and CO_2, achieving a remarkable CO_2 detection limit of 500 ppm at a 200 s integration time—fully meeting industrial emission monitoring requirements.

Author Contributions: Methodology, Formal analysis, Writing—original draft preparation, M.F.; Conceptualization, Writing—review and editing, Supervision, Funding acquisition, H.Y.; Conceptualization, Writing—review and editing, Supervision, Funding acquisition, J.C. All authors have read and agreed to the published version of the manuscript.

Funding: This research was funded by the National Natural Science Foundation of China (grant Nos. 52376161).

Data Availability Statement: The data presented in this study are available upon request from the corresponding author.

Acknowledgments: The authors would like to extend special thanks to Xiaofan Yang for his invaluable advice and support in experimental techniques, which greatly facilitated the experiments.

Conflicts of Interest: The authors declare no conflicts of interest.

References

1. Kreuzer, L.B. Ultralow gas concentration infrared absorption spectroscopy. *J. Appl. Phys.* **1971**, *42*, 2934–2943. [CrossRef]
2. Rosencwaig, A. New tool for investigation of solids. *Anal. Chem.* **1975**, *47*, 592A–604A. [CrossRef]
3. Berden, G.; Peeters, R.; Meijer, G. Cavity ring-down spectroscopy: Experimental schemes and applications. *Int. Rev. Phys. Chem.* **2000**, *19*, 565–607. [CrossRef]
4. Crosson, E.R.; Ricci, K.N.; Richman, B.A.; Chilese, F.C.; Owano, T.G.; Provencal, R.A.; Todd, M.W.; Glasser, J.; Kachanov, A.A.; Paldus, B.A.; et al. Stable isotope ratios using cavity ring-down spectroscopy: Determination of 13C/12C for carbon dioxide in human breath. *Anal. Chem.* **2002**, *74*, 2003–2007. [CrossRef]
5. Murphy, M.S.; Sood, M.; Johnson, T. Use of the lactose H2 breath test to monitor mucosal healing in coeliac disease. *Acta Paediatr.* **2002**, *91*, 141–144.
6. Barik, P.; Pradhan, M. Selectivity in trace gas sensing: Recent developments, challenges, and future perspectives. *Analyst* **2022**, *147*, 1024–1054. [CrossRef]
7. Smekal, A. Zur quantentheorie der dispersion. *Naturwissenschaften* **1923**, *11*, 873–875. [CrossRef]
8. Raman, C.V.; Krishnan, K.S. A new type of secondary radiation. *Nature* **1928**, *121*, 501–502. [CrossRef]
9. Wang, P.; Chen, W.; Wan, F.; Wang, J.; Hu, J. A review of cavity-enhanced Raman spectroscopy as a gas sensing method. *Appl. Spectrosc. Rev.* **2020**, *55*, 393–417. [CrossRef]
10. Wang, P.; Wan, F.; Wang, J.; Chen, W.; Zhu, C.; Liu, Y. Injection-locked cavity-enhanced Raman spectroscopy for trace gas detection technology. *Opt. Precis. Eng.* **2018**, *26*, 1917–1924. [CrossRef]
11. Colthup, N. *Introduction to Infrared and Raman Spectroscopy*; Elsevier: Amsterdam, The Netherlands, 2012.
12. Wackerbarth, H.; Salb, C.; Gundrum, L.; Niederkrüger, M.; Christou, K.; Beushausen, V.; Viöl, W. Detection of explosives based on surface-enhanced Raman spectroscopy. *Appl. Opt.* **2010**, *49*, 4362–4366. [CrossRef] [PubMed]
13. Krafft, C.; Dietzek, B.; Schmitt, M.; Popp, J. Raman and coherent anti-Stokes Raman scattering microspectroscopy for biomedical applications. *J. Biomed. Opt.* **2012**, *17*, 040801. [CrossRef] [PubMed]
14. Arismar Cerqueira, S., Jr.; Luan, F.; Cordeiro, C.M.B.; George, A.K.; Knight, J.C. Hybrid photonic crystal fiber. *Opt. Express* **2006**, *14*, 926–931. [CrossRef] [PubMed]

15. Sandfort, V.; Goldschmidt, J.; Wöllenstein, J.; Palzer, S. Cavity-enhanced Raman spectroscopy for food chain management. *Sensors* **2018**, *18*, 709. [CrossRef]
16. Ismail, N.; Kores, C.C.; Geskus, D.; Pollnau, M. Fabry-Pérot resonator: Spectral line shapes, generic and related Airy distributions, linewidths, finesses, and performance at low or frequency-dependent reflectivity. *Opt. Express* **2016**, *24*, 16366–16389. [CrossRef]
17. Claps, R.; Sabbaghzadeh, J.; Fink, M. Raman spectroscopy with a single-frequency, high-power, broad-area laser diode. *Appl. Spectrosc.* **1999**, *53*, 491–496. [CrossRef]
18. Hill, R.A.; Mulac, A.J.; Hackett, C.E. Retroreflecting multipass cell for Raman scattering. *Appl. Opt.* **1977**, *16*, 2004–2006. [CrossRef]
19. Kc, U.; Silver, J.A.; Hovde, D.C.; Varghese, P.L. Improved multiple-pass Raman spectrometer. *Appl. Opt.* **2011**, *50*, 4805–4816. [CrossRef]
20. Li, X.-Y.; Xia, Y.-X.; Huang, J.M.; Zhan, L. Diagnosis of multiple gases separated from transformer oil using cavity-enhanced Raman spectroscopy. *Chin. Phys. Lett.* **2008**, *25*, 3326.
21. Li, X.Y.; Xia, Y.X.; Huang, J.M.; Zhan, L. A Raman system for multi-gas-species analysis in power transformer. *Appl. Phys. B Laser Opt.* **2008**, *93*, 665–669. [CrossRef]
22. Hippler, M.; Mohr, C.; Keen, K.A.; McNaghten, E.D. Cavity-enhanced resonant photoacoustic spectroscopy with optical feedback cw diode lasers: A novel technique for ultratrace gas analysis and high-resolution spectroscopy. *J. Chem. Phys.* **2010**, *133*, 044308. [CrossRef] [PubMed]
23. Yokoyama, H.; Nishi, K.; Anan, T.; Nambu, Y.; Brorson, S.D.; Ippen, E.P.; Suzuki, M. Controlling spontaneous emission and threshold-less laser oscillation with optical microcavities. *Opt. Quantum Electron.* **1992**, *24*, S245–S272. [CrossRef]
24. Velez, J.G.; Muller, A. Trace gas sensing using diode-pumped collinearly detected spontaneous Raman scattering enhanced by a multipass cell. *Opt. Lett.* **2020**, *45*, 133–136. [CrossRef]
25. Cox, A.J.; DeWeerd, A.J.; Linden, J. An experiment to measure Mie and Rayleigh total scattering cross sections. *Am. J. Phys.* **2002**, *70*, 620–625. [CrossRef]
26. Sheppard, N. The historical development of experimental techniques in vibrational spectroscopy. In *Handbook of Vibrational Spectroscopy*; John Wiley & Sons, Ltd.: Hoboken, NJ, USA, 2006.

Disclaimer/Publisher's Note: The statements, opinions and data contained in all publications are solely those of the individual author(s) and contributor(s) and not of MDPI and/or the editor(s). MDPI and/or the editor(s) disclaim responsibility for any injury to people or property resulting from any ideas, methods, instructions or products referred to in the content.